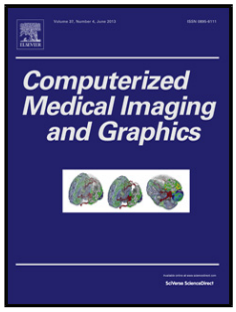

Title: Automatic Detection of Microaneurysm in Retinal Fundus Images

Author: Bo Wu Weifang Zhu Fei Shi Shuxia Zhu Xinjian Chen

PII: S0895-6111(16)30078-7
DOI: http://dx.doi.org/doi:10.1016/j.compmedimag.2016.08.001
Reference: CMIG 1464

To appear in: *Computerized Medical Imaging and Graphics*

Received date: 31-1-2016
Revised date: 22-7-2016
Accepted date: 3-8-2016

Please cite this article as: Wu Bo, Zhu Weifang, Shi Fei, Zhu Shuxia, Chen Xinjian.Automatic Detection of Microaneurysm in Retinal Fundus Images.*Computerized Medical Imaging and Graphics* http://dx.doi.org/10.1016/j.compmedimag.2016.08.001

Automatic Detection of Microaneurysm in Retinal Fundus Images

Bo Wu, Weifang Zhu, Fei Shi, Shuxia Zhu, Xinjian Chen*

School of Electronic and Information Engineering, Soochow University, Suzhou, China

This work was supported by the National Basic Research Program of China (973 Program) under Grant 2014CB748600.

*Corresponding author. Tel.: +8618260180695
E-mail address: xjchen@suda.edu.cn (Xinjian Chen)

Highlights

- An automatic method for detection of microaneurysms in fundus images is proposed.
- Several effective prepocessing steps are applied to make a suitable image for candidate extraction and feature extraction.
- A total of 27 important features are extracted to describe a MA. These features can be divided in to local features and profile features. The local features are extracted by the way that we see a MA and its surroundings as a whole. And, the profile features are extracted by the way we see a MA from its 20 profiles.
- Several classifiers are selected to find a suitable classifier for the proposed feature set.

Abstract

Diabetic retinopathy (DR) is one of the leading causes of new cases of blindness. Early and accurate detection of microaneurysms (MAs) is important for diagnosis and grading of diabetic retinopathy. In this paper, a new method for the automatic detection of MAs in eye fundus images is proposed. The proposed method consists of four main steps: preprocessing, candidate extraction, feature extraction and classification. A total of 27 characteristic features which can be divided into local features and profile features are extracted for classifier to distinguish true MAs from spurious candidates. Furthermore, three classifiers such as K-Nearest Neighbor, Naïve Bayes and Adaboost are selected as the underlying classifier to find a suitable classifier for the feature set. The proposed method has been evaluated on two public database: e-optha and ROC. the result shows that the proposed method is very effective and has the potential to help diagnose DR.

Keywords: microaneurysms (MAs), diabetic retinopathy (DR), local features, profile features, classifier, eye fundus images.

1. Introduction

Diabetic retinopathy (DR) is one of the main complications caused by diabetes. It is reported that DR has been the leading cause of new cases of blindness among adults aged between 20 and 74 years old [1]. According to the World Health Organization (WHO), 347 million people were diagnosed with diabetes worldwidely [2]. It is also predicted that, by 2040, more than 640 million people may be living with diabetes [3].

In general, DR can be classified into two types, non-proliferative diabetic retinopathy (NPDR) and proliferative diabetic retinopathy (PDR) [4], or six stages by the presence of different signs in retina. Most of the damage caused by DR can be reduced or prevented if it is diagnosed appropriately and regularly at the early stages.

However, it is impractical to conduct that work for all the diabetic patients by ophthalmologists manually. Except for time-consuming, human error and a lack of ophthalmologists are other two important reasons. Hence, automatic analysis of diabetic patients' retina is required for ophthalmologists to screen larger populations of patients.

Microaneurysms (MAs) appear as small and round shape dots near tiny blood vessels in fundus images. They are likely to be the only lesion, which present at the earliest stage of DR and remain in the development of disease [5, 6]. Therefore, detection of MAs is necessary and vital in a computer-aided screening system.

Analysis of eye fundus images is one of common clinical procedures in diagnosis of DR. To compare with fluorescein angiography (FA), the acquisition of the fundus images is fast, cheap and non-invasive [7-10]. Besides, the FA is not applicable for everyone, such as the pregnant woman [11-12]. Thus, adaption of the eye fundus images is the better choice for screening purpose. Fig.1 shows a fundus image with several MAs.

The diameter of MAs usually ranges from 10 μm to 100 μm [13], which is considered less than the diameter of the major optic veins. Some objects of eye fundus images are similar to MAs in size and shape, which makes it difficulty to recognize MAs from them. One kind of them are small and round spots resulted from crossing of thin blood vessels. In fact, MAs can not lie on the vessels. In addition, vessel segments can also increase the difficulty of identifying MAs in fundus images, which appear as dark, small objects of various shapes.

In [14], Baudoin and Lay *et al*. proposed a computerized approach for detection of MAs in fluorescein angiograms, which used mathematical morphology. The MAs were extracted from the FA by using different top-hat transformations. However, as discussed above, the FA is not suitable for screening systems. Besides, the method is very time consuming. The conception of mathematical morphology was also applied in [15]. The MA candidates were extracted by removing vessels and small objects using canny edge detection and region filling algorithm. A post processing step was used to remove useless objects. Accurate detection of MAs was dependent on accurate detection of blood vessels and optic disc in this method. Spencer *et al*. [16] proposed a method for detection of MAs using adaptive filters. Several features about intensity, size and shape of MA candidates were calculated. The disadvantages of the method are that it uses FA images and is sensitive to the resolution of the FA images. Niemeijer *et al*. [17] proposed a novel red lesion detection method based on a hybrid approach, which incorporated the previous works of Spencer *et al*. [16] and Frame *et al*. [18] with two new contributions. However, the total time of the method to process

a single image is about 15 minutes, which is too long for screening systems. In [19], image contrast normalization was used to improve the ability to distinguish MAs from other dots in fundus image. The average execution time per image goes from 53s to 100s. However, the sensitivity and specificity of the method are a little low for an efficient diagnostic tool. Template matching in the wavelet domain was proposed for detection of MAs in [20]. By choosing appropriate sub-bands, the problems caused by illumination or high-frequency noise can be solved well without other image processing. In [21], Antal proposed a novel ensemble-based system for MA detection and diabetic retinopathy grading. They improved MA detection by selecting the optimal combination of preprocessing methods and candidate extractors. An artificial neural network (ANN) [22] was applied to recognize objects of diabetic fundus images, such as MAs, vessels and exudates. Convolution neural network (CNN) is a kind of artificial neural network. It is generally considered suitable for image recognition. The method was applied for detecting MAs by Haloi [23] and achieved a sensitivity of 97% and a specificity of 95%. The disadvantage of these methods are the requirement for a large amount of training data and time-consuming. Lazar [24] proposed a method for automatic detection of MAs through local rotating cross-section profile analysis. The local maximum pixels were selected as candidates. The cross-sectional scanning was applied to each candidate to produce 30 profiles. Then, peak detection was applied on each profile, and 7 properties of the peak is calculated. Several statistical measures of the resulting directional peak properties are as the set of features for a Bayesian classifier.

In this paper, we propose a novel MA detection method base on Lazar's method with two new important contributions. (1) Region growing is considered in the proposed method to grow preliminary candidate pixels back to the original pathologies. Additional postprocessing step is used to eliminate false preliminary

candidates; (2) Except for 3 new profile features, 17 local features are extracted to describe the MA.

The rest of this paper is organized as follows. Section 2 describes the step of the proposed method in details. In section 3, the experimental results are present. Conclusion and discussion are presented in section 4.

2. Proposed method

2.1 Overview of the method

In this method , the inverted-green channel of fundus images is used as main input. The green channel provides the best MA-background contrast, while red channel is saturated. Blue channel is the darkest color channel and does not contain any information. Walter T [1] explained why the green channel contains most of the image information. The binary region of interest (ROI) mask is also considered. The input images are required to have such spatial resolution that the diameter of their ROI is equal to 920 pixels. In fact, the proposed method can be applied on images of different spatial resolution by setting corresponding parameters.

The pipeline of the method presented in this paper is illustrated in Fig. 2. Firstly, some necessary steps of preprocessing are adopted to make MAs more visible. Secondly, the MA candidate regions are identified in the preprocessed image, based on the peak detection and region growing. Thirdly, several features are extracted for classification. Lastly, several classfiers are modified to distinguish true MAs from spurious candidates.

2.2 Image preprocessing

Retinal fundus images are often nonuniform illumination, poor contrast and noise. MAs are hardly visible in regions of low brightness and poor contrast. In order to reduce these drawbacks and make a suitable image for MA candidate extraction and feature extraction, three preprocessing steps are applied as follow:

2.2.1 Illumination Equalization

The illumination equalization method in [25] is used to correct shade as follows:

$$I_{ie} = I - I_{bg} + u\,. \qquad (1)$$

A mean filter of size 51*51 is applied to the original green channel image I to generate a background image I_{bg}, which is used to estimate its illumination. Then, the I_{bg} is subtracted from the I to correct for shade variations. Lastly, the average intensity u of I is added to keep the same gray range as in the I.

2.2.2 Contrast Limited Adaptive Histogram Equalization (CLAHE)

In general, many MAs in the original inverted green-channel fundus images do not have enough contrast with the surrounding background, which affect the next

detection steps. Therefore, an enhancement method of contrast limited adaptive histogram equalization (CLAHE) [26] is applied to solve this problem. The enhancement technique is widely used in biomedical image processing and can make the interesting salient parts more visible effectively.

2.2.3 Smoothing

Most of the available fundus images are stored in a lossy compressed form, which make small structures such as MAs distorted. That is not conducive to extract extremely characteristic features of MAs. In addition, due to the small size of MAs, it is important to reduce the effect of noise. Thus, it is necessary to consider of a mountain of image smoothing before actual steps of detection. In our implementation, a Gaussian filter with a width of 7 and a variance of 1.0 was applied. The Fig. 3 shows an original inverted green-channel fundus image and the resulting images processed by above steps.

2.3 Candidate extraction

The step of candidate extraction plays an important role in the whole detection. One side, the main objective of this step is to reduce the number of objects which is not similar to MAs. On the other side, any true MAs lost in this step can not be retrieved later. In this paper, the preliminary candidates are extracted by profile analysis which is described in [24]. As MAs appear as bright structures in the preprocessed image, the MA region contains at least one regional maximum. Thus, the local maximum pixels can be considered as MA candidates. However, a large amount of noise will be extracted in this way. In order to overcome this limitation, peak detection is applied on each profile. Fig. 4 shows the intensity distribution of a profile, which the candidate pixel is located in the center. After peak detection, the peak can be represented by four descriptive values: IR_s , IR_e , DR_s and DR_e . In our implementation, 20 line detectors with 9° angular resolution are applied to generate 20 profiles. If any of the profiles which has no absolute difference between consecutive pixels larger than 5, the candidate is eliminated. The enhancement of CLAHE gains importance at this point. The method of CLAHE helps profile analysis to eliminate most noise due to the fact that it can enhance the contrast of MA while suppress the noises.

The preliminary candidates can not represent the pathologies as found in the original retinal fundus image. Region growing is often used to grow MA candidates

back to the original pathologies in candidate extraction step [16-17, 19]. However, the growing threshold is hard to determined due to the variable intensity and size of MAs. In order to overcome this problems, the dynamic transformation [27] which valuates the regional maximum on a contrast criterion is applied.

If the preprocessed image is seen as a topographic surface, the dynamic of a local maximum is calculated as the difference in intensity between the given maximum and lowest pixel of the paths reaching a maximum of higher intensity. The original aspect of this definition is that it does not consider the size and shape of the regional maximum. An adaptive threshold t based on the dynamics can be calculated for region growing as follows:

$$t = i_{seed} - \beta * d_{seed} \qquad (2)$$

where i_{seed} is the intensity of the starting position in the preprocessed image. In this paper, they are the preliminary candidate pixels. The d_{seed} is the dynamic value and $\beta \in (0,1]$. Here, $\beta = 0.53$. Growing starts in the seed pixel and stops when there are no connected pixels higher than the threshold. Considering the MA's size is limited, every resultant connected component, which is lager than 140, will be discarded. In addition, elongated structures which are probably vessels can be discarded by area ratio r, which is calculated as follows:

$$r = \frac{S_{cand}}{S_{circle}} \qquad (3)$$

where S_{cand} is the area of the candidate and S_{circle} is the area of the candidate's circumcircle. The connected components will be also discarded , whose r is smaller than 0.5.

2.4 Feature extraction

The features proposed by Lazar are derived from profile analysis. In this paper, we define these features as profile features. But these profile features can not reflect overall characteristics of MAs well. Therefore, we also see a MA and its surroundings as a whole and several overall features are extracted. We call these features as local features. Besides, 3 new profile features are also proposed in this paper.

2.4.1 Local features

2.4.1.1 Hessian matrix based features

The Hessian matrix is square matrix of second-order partial derivatives of a scalar-valued function. It describes the local curvature of a function of many variables. Hessian matrix in 2D images is taken by second partial derivative from image's pixel and given as

$$H(x,y)=\begin{bmatrix} D_{xx} & D_{xy} \\ D_{xy} & D_{yy} \end{bmatrix} \tag{4}$$

$$D_{xx}=G_{xx}(x,y;\sigma)*I(x,y) \tag{5}$$

$$D_{xy}=G_{xy}(x,y;\sigma)*I(x,y) \tag{6}$$

$$D_{yy}=G_{yy}(x,y;\sigma)*I(x,y) \tag{7}$$

Where $I(x,y)$ is the preprocessed image, * is convolution operator, and G_{xx}, G_{xy}, and G_{yy} are second-order Gaussian derivative along each direction.

Alejandro F. Frangi [28] summarizes the relations that must hold between the eigenvalues of the Hessian matrix for the detection of different structures. Let λ_1 and λ_2 be two eigenvalues ($|\lambda_1|\le|\lambda_2|$) . Because MAs appear as small, round and bright objects in preprocessed images, a MA-like probability map can be established by

$$P_M(x,y;\sigma)=\begin{cases} 0 & \lambda_1>0 \,||\, \lambda_2>0 \\ \frac{2}{\pi}\arctan\left(\frac{|\lambda_2|+|\lambda_1|}{|\lambda_2|-|\lambda_1|}\right) & \lambda_1\neq\lambda_2 \\ 1 & \lambda_1=\lambda_2<0 \end{cases} \tag{8}$$

$$P_M(x,y)=\max_{\sigma_{\min}<\sigma<\sigma_{\max}} P_M(x,y;\sigma) \tag{9}$$

When P_M has a large value, the possibility of the pixel(x,y) belonging to a MA is high.

For each candidate regions, the following features are extracted:

- Mean of P_M, $|H|$
- Max of P_M, $|H|$
- Standard deviation of P_M, $|H|$

Here, $|H|=\lambda_{1M}*\lambda_{2M}$. λ_{1M} and λ_{2M} are the eigenvalues when P_M achieves the maximum. A total of 6 features are extracted.

2.4.1.2 Shape and intensity features

For extracting intensity and shape features, a sub-ROI is considered. The sub-ROI is nine times as large as the candidate region. The candidate region is located in the center of sub-ROI and the remaining region is as background. Besides, the shape of the sub-ROI is circular because MAs appear as round structure in the fundus images.

For each candidate region, the following shape and intensity features are extracted:

(1) The area $S = \sum_{j \in \Omega} 1$, where Ω is the set of pixels in the candidate region.

(2) The symmetry $R = \frac{\sum \sqrt{(d - \bar{d})^2}}{n}$, where d is the distance from a edge pixel to the darkest pixel (center pixel) of the candidate region. The $\bar{d}$ is the mean distance.

(3) The aspect ratio $P = \frac{l}{w}$, where l is the length of the largest and w is the second largest eigenvalue of the convariance matrix of the candidate region.

(4) The mean contrast of edge pixels. The contrast of a pixel can be calculated by $C = \frac{\sum_{j \in \mathrm{A}} g_j}{N_{\mathrm{A}}} - \frac{\sum_{j \in \mathrm{B}} g_j}{N_{\mathrm{B}}}$, where A is a set of pixels which belong to the 8-neiboring pixels of the calculated pixel and their intensity is greater or equal to calculated pixel. N_{A} is the number of pixels belonging to A. B is the remaining pixels of 8-neiboring pixel.

(5) The standard deviation of edge pixels' contrast $\sigma_C = \frac{\sum_{j \in \mathrm{Z}} \sqrt{(C_j - \bar{C})^2}}{N_Z}$, where Z is a set of edge pixels and N_Z is the number of these pixels.

(6) The mean intensity of MA candidate region $M_{cand} = \frac{\sum_{j \in \Omega} g_j}{N}$.

(7) The standard deviation of MA candidate region intensity $\sigma_{cand} = \frac{\sum_{j \in \Omega} \sqrt{(g_j - M_{obj})^2}}{N}$.

(8) The mean intensity of background $M_{bg} = \frac{\sum_{j \in \mathrm{E}} g_j}{N_{bg}}$, where E is a set of pixels belonging to background. Considering the thick vessel may affect intensity distribution of background, which corresponding MA candidate is near the thick

vessel. That may affect the detection. The background has removed the pixels whose intensity are lower the MA candidate's darkest one.

(9) The standard deviation of background intensity $\sigma_{bg} = \frac{\sum_{j \in \mathrm{E}} \sqrt{(g_j - M_{bg})^2}}{N_{bg}}$.

(10) The difference between the mean intensity of MA candidate and its background $M_{diff} = M_{bg} - M_{obj}$.

(11) The difference between the maximal intensity of candidate region and a local contrast $D = g_{\max} - t$, where $t = M_{bg} - \beta\sqrt{\sigma_{bg}}$. It gives additional information about gray difference between MA candidate and its surroundings.

2.4.2 Profile features

A total of 7 different profile features were proposed by Lazar [24]. In this paper, several new profile features were proposed to improve performance. For better understanding, some necessary properties of the profile are also described here as follows:

1) The mountain width is the difference between the start and end of the peak: $W_{peak} = DR_e - IR_s$.

2) The *increasing ramp height*: $H_{IR} = P[IR_e] - P[IR_s]$.

3) The *decreasing ramp height*: $H_{DR} = P[DR_s] - P[DR_e]$.

4) The *mean height* of the peak: $\overline{H_{peak}} = \sum_{IR_s}^{DR_e} P[i] / W_{peak}$.

5) The *start of increasing ramp height*: $H_{IR_s} = P[IR_s]$.

6) The *end of the decreasing ramp height*: $H_{DR_e} = P[DR_e]$.

The properties of 4 to 6 are new proposed in this paper to extract new features. After a whole peak detection finishes, every property set stores 20 values in this paper. Then, 3 new sets are defined to store these values for better understanding. The start of the increasing ramp and the end of the decreasing ramp height values are stored in FHEIGHT set, likewise, mean height of the peak is stored in the MPHEIGHT. The PHEIGHT stores the increasing and decreasing ramp height. Let σ_T denotes standard deviation of the values in set *T*. Thus, 2 new features can be acquired by calculating $\sigma_{\overline{H_{peak}}}$ and $\sigma_{FHEIGHT}$. This two features provide more information about how symmetric the candidate is. The 3rd feature is adopted to help

eliminate the candidates located in blood vessels. Let $\max_{height}$ and $\min_{height}$ donate the max value and min value of MHEIGHT set, respectively. The feature is calculated as $R_{height} = (\max_{height} - \min_{height}) / \min_{height}$. The candidates located in the vessel have large R_{height} than the true MAs.

In summary, a total of 27 features (6 Hessian matrix + 11 shape and intensity + 10 profile) have been extracted for each candidate.

2.6 Classification

In the stage of feature extraction, each MA candidate is characterized by a vector in a 27-D feature set

$$F = \{f_1, f_2, ..., f_{27}\}. \quad (10)$$

However, the different feature f_i have different ranges and values, which is not good for some classifiers. Each of these features is normalized to zero mean and unit variance by applying

$$\overline{f_i} = \frac{f_i - \mu_i}{\sigma_i} \quad (11)$$

where μ_i is the mean of the i th feature, and σ_i is its standard deviation. In order to select suitable classifier for the feature set, four supervised classifier are selected as the underlying classifiers: K-Nearest Neighbor (KNN), Naïve Bayes (NB) and Adaboost.

3. Result

3.1 Database

The proposed method has been tested on two public available database: e-ophtha and Retinopathy Online Challenge (ROC) database.

The e-ophtha is collected by E.Decencière and made of two sub databases called e-ophtha-MA (Microaneurysms) and e-ophtha-EX (Exudates). E-ophtha-MA comprises 148 fundus images with microaneurysms or small hemorrhages, which manually annotated by ophthalmology experts. In this paper, 74 fundus images are used as training set and the remaining 74 fundus images as test set.

The ROC is a competition which aims to help patients with diabetes through improving computer aided detection. The ROC database is made up of 50 images for training and 50 images for testing. However, only the annotations of training set are

public. Besides, Only 37 images of training set contain MAs, while the other 13 images do not contain any MA. Thus, the 10-fold cross-validation was applied to evaluate the ability of classifiers when we use this database.

3.2 Assessment of classification performance

It is often not sufficient to simply detect the existence of MAs. Correct localization of the MAs is required for a true-positive detection. Therefore, in this paper, the free-response ROC (FROC) is used to evaluated the classification performance [29]. An FROC curve is a polt of operating points displaying the possible tradeoff between the sensitivity vs the average number of false positive detection per image. The sensitivity is calculated as follows:

$$sensitivity = \frac{TP}{TP + FN} \tag{12}$$

where TP denotes true positive and FN denotes false negative.

The ROC database is used to evaluate the three classifiers. The corresponding FROC curves of classification results is plotted in Fig. 5. The evaluation results show that the KNN and Adaboost classifiers have similar performance and both outperform the NB classifier. The proposed method is also compared with Lazar's method on the ROC database. Both methods use the best performing classifier of KNN. Fig. 6 shows the FROC curve of the proposed method and Lazar's method. Table Ⅰshows the sensitivities at seven false positive rates (1/8, 1/4, 1/2, 1, 2, 4 and 8 false positives per image) for the proposed method and Lazar's method. The final score of a method is calculated as the average sensitivity at the seven false positive rates. Our method achieves an overall score of 0.202, which is better than 0.152 of Lazar's method.

The performance of the proposed method has also been evaluated on a publicly available database e-ophtha-MA. The FROC curve is shown in Fig. 7 and corresponding seven sensitivities are shown in Table Ⅱ. The score of the proposed method achieved 0.273 on this database.

4. Discussion and conclusion

In this paper, we have proposed a method for automatic detection of MAs in fundus images. Several preprocessing steps are applied to generate suitable images for candidate extraction and feature extraction. The preliminary candidate pixels are

extracted by the profile analysis which is described in [24]. At this point, an advantage of our method is that we have added image enhancement step in the preprocessing step. The enhancement method of CLAHE have a good performance on making MA more visible whiel suppressing noises. Eventually, the enhancement makes the profile analysis eliminate more noise. The region growing is adopted to grow preliminary candidate pixels back to original pathologies. The dynamic, a measure of contrast, is applied to calculate adaptive growing threshold. After that, two additional postprocessing steps can further eliminate preliminary candidates, which are larger than 140 pixels or appear as elongated structures. Except the 7 profile features which is proposed by Lazar, 20 new features are proposed in this paper. 17 of 20 feature are base on MA local information and the remaining 3 feature are new profile features. For classification, three classifiers of K-Nearest Neighbor (KNN), Naïve Bayes (NB) and Adaboost are tested to find a suitable classifier for our feature set.

The proposed method has been evaluated in two public database: e-ophtha and ROC. The results show that the KNN and Adaboost classifiers have similar classification performance and outperform Naïve Bayes classifier. The proposed method is also compared with the method of Lazar. The result shows that our method has a better performance.

In summary, a fully and automated and efficient methodology is proposed for detection of MAs. The proposed method is proved to outperform Lazar' method. We believe this method has the potential to be used in diabetic retinopathy screen system.

5. References

[1] Walter T, Massin P, Erginay A, et al. Automatic detection of microaneurysms in color fundus images. Medical Image Analysis 2007; 11(6):555–566.

[2] World Health Organization (WHO) [Online] http://www.who.int/features/factfiles/diabetes/facts/zh/

[3] International Diabetes Federation [Online] http://www.idf.org/wdd-index/

[4] Zhang B, Wu X, You J, et al. Detection of microaneurysms using multi-scale correlation coefficients. Pattern Recognition 2010; 43(6):2237–2248.

[5] Early Treatment Diabetic Retinopathy Study Research Group. Early photocoagulation for diabetic retinopathy. Ophthalmology 1991; vol. 98, pp. 766–85.

[6] Antal B, Hajdu A. Improving microaneurysm detection using an optimally selected subset of candidate extractors and preprocessing methods. Pattern Recognition 2012; 45(1):264-270.

[7] Hipwell J H, Strachan F ,, Olson J A, et al. Automated detection of microaneurysms in digital red-free photographs: a diabetic retinopathy screening tool. Diabetic Medicine A Journal of the British Diabetic Association 2000; 17(8):588-594.

[8] Michael L, Jannik G, Nicolai L, et al. Automated detection of fundus photographic red lesions in diabetic retinopathy. Investigative Ophthalmology & Visual Science 2003; 44(2):761-6.

[9] Thanh W. A contribution of image processing to the diagnosis of diabetic retinopathy detection of exudates in color fundus images of the human retina. IEEE Transactions on Medical Imaging 2002; 21(10):1236-43.

[10] Sinthanayothin C, Boyce J F, Williamson T H, et al. Automated detection of diabetic retinopathy on digital fundus images. Diabetic Medicine 2002; 19(2):105–112.

[11] Frame A J, Undrill P E, Cree M J, et al. A comparison of computer based classification methods applied to the detection of microaneurysms in ophthalmic fluorescein angiograms. Computers in Biology & Medicine 1998; 28(3):225-238.

[12] Mendon&#, A, A M, Campilho A J, et al. Automatic Segmentation of Microaneurysms in Retinal Angiograms of Diabetic Patients. IEEE 1999;728-733.

[13] Pereira C, Veiga D, Mahdjoub J, et al. Using a multi-agent system approach for microaneurysm detection in fundus images. Artificial Intelligence in Medicine 2014; 60(3):179–188.

[14] Baudoin C E, Lay B J, Klein J C. Automatic detection of microaneurysms in diabetic fluorescein angiography. Revue D Épidémiologie Et De Santé Publique 1984; 32(3-4):254-61.

[15] Purwita A A, Adityowibowo K, Dameitry A, et al. Automated microaneurysm detection using mathematical morphology. Instrumentation, Communications, Information Technology, and Biomedical Engineering (ICICI-BME), 2011 2nd International Conference on. IEEE 2011;117-120.

[16] Spencer T ,, Phillips R P, Sharp P F, et al. Automated detection and quantification of microaneurysms in fluorescein angiograms. Albrecht Von Graæes Archiv Für Ophthalmologie 1992; 230(1):36-41.

[17] Meindert N, Bram V G, Joes S, et al. Automatic detection of red lesions in digital color fundus photographs. IEEE Transactions on Medical Imaging 2005; 24(5):584-92.

[18] Frame A J, Undrill P E, Cree M J, et al. A comparison of computer based classification methods applied to the detection of microaneurysms in ophthalmic fluorescein angiograms. Computers in Biology & Medicine 1998; 28(3):225-238.

[19] Fleming A D, Sam P, Goatman K A, et al. Automated microaneurysm detection using local contrast normalization and local vessel detection. IEEE Transactions on Medical Imaging 2006; 25(9):1223-1232.

[20] Gwénolé Q, Mathieu L, Pierre Marie J, et al. Optimal wavelet transform for the detection of microaneurysms in retina photographs. IEEE Transactions on Medical Imaging 2008; 27(9):1230-41.

[21] Antal B, Hajdu A. An Ensemble-Based System for Microaneurysm Detection and Diabetic Retinopathy Grading. Biomedical Engineering, IEEE Transactions on 2012; 59(6):1720-1726.

[22] Gardner G G, Keating D, Williamson T H, et al. Automatic detection of diabetic retinopathy using an artificial neural network: A screening tool. British Journal of Ophthalmology 1996; 80(11):940-4.

[23] Mrinal Haloi, "Improved Microaneurysm Detection using Deep Neural Networks," [online] http://arxiv.org/abs/1505.04424

[24] Istvan L, Andras H. Retinal Microaneurysm Detection Through Local Rotating Cross-Section Profile Analysis. IEEE Transactions on Medical Imaging 2013; 32(2):400-407.

[25] Hoover A, Goldbaum M. Locating the optic nerve in a retinal image using the fuzzy convergence of the blood vessels.[J]. IEEE Transactions on Medical Imaging, 2003, 22(8):951-8.

[26] Zuiderveld K. Contrast Limited Adaptive Histogram Equalization[J]. Graphics Gems, 1994:474-485.

[27] Grimaud M. New measure of contrast: the dynamics[J]. Image Algebra & Morphological Image Processing III, 1992:292-305.

[28] Alejandro F. Frangi, Wiro J. Niessen, Koen L. Vincken and Max A. Viergever. Multiscale Vessel Enhancement Filtering[J]. Lecture Notes in Computer Science, 2000, 1496:130-137.

[29] Bunch P C, Hamilton J F, Sanderson G K, et al. A Free Response Approach To The Measurement And Characterization Of Radiographic Observer Performance. Proc Spie 1977; 4(4).

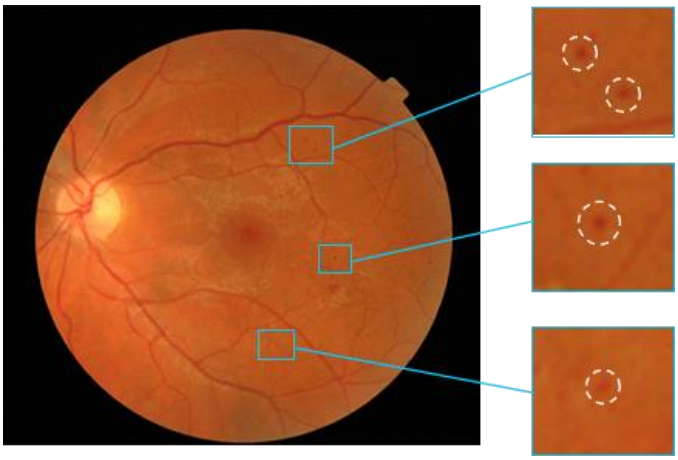

Fig. 1. An example of a fundus image with several MAs.

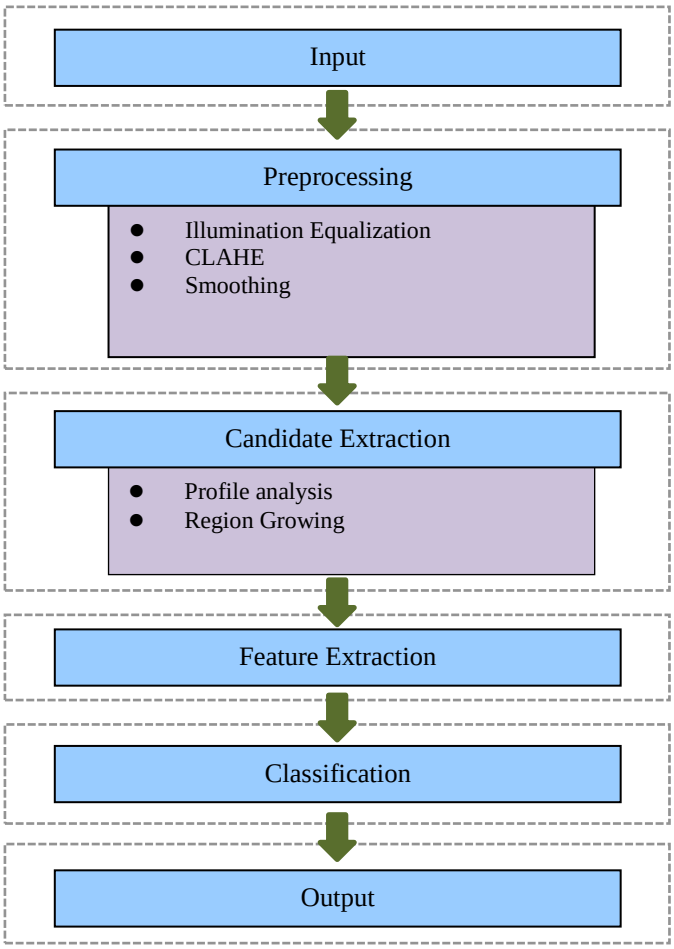

Fig. 2. Flowchart of the proposed method.

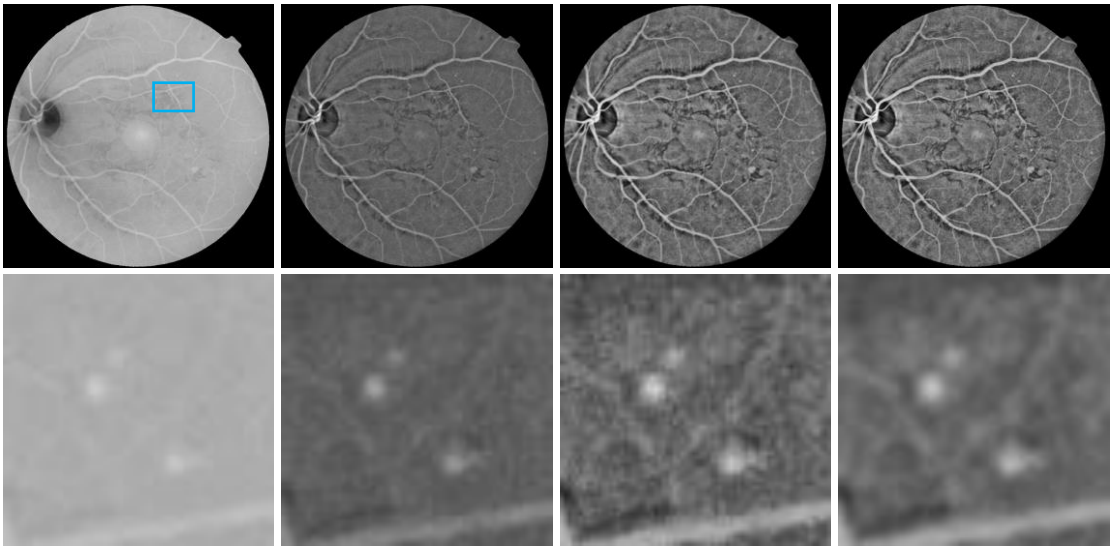

(a) I (b) I_{ie} (c) I_{en} (d) I_p

Fig. 3. The illustration of preprocessing steps. (a) Original inverted green-channel image I ; (b) illumination equalization I_{ie} ; (c) contrast limited adaptive histogram equalization enhancement image I_{en} ; (d) the resulted image I_p after the step of smoothing. The lower row shows the details in blue rectangle after each steps.

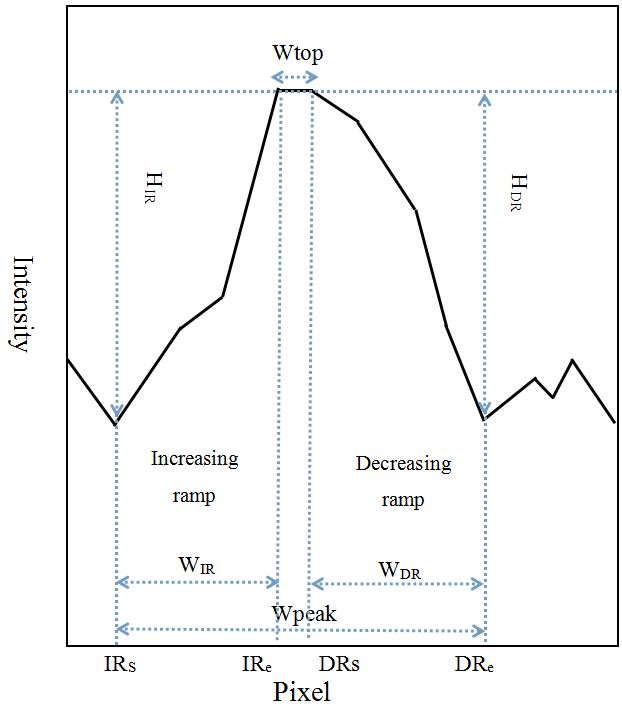

Fig. 4. The intensity distribution of a profile and the definitions of the peak.

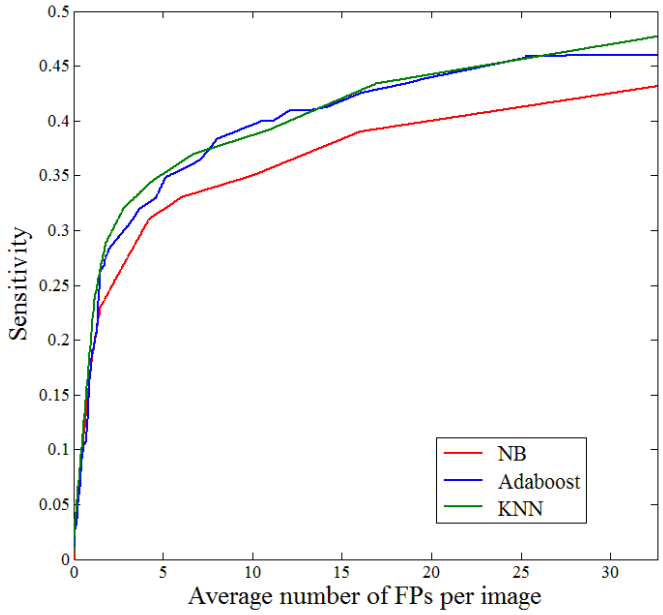

Fig. 5. The FROC curves of classification results by applying the KNN, NB and Adaboost classifiers to ROC database.

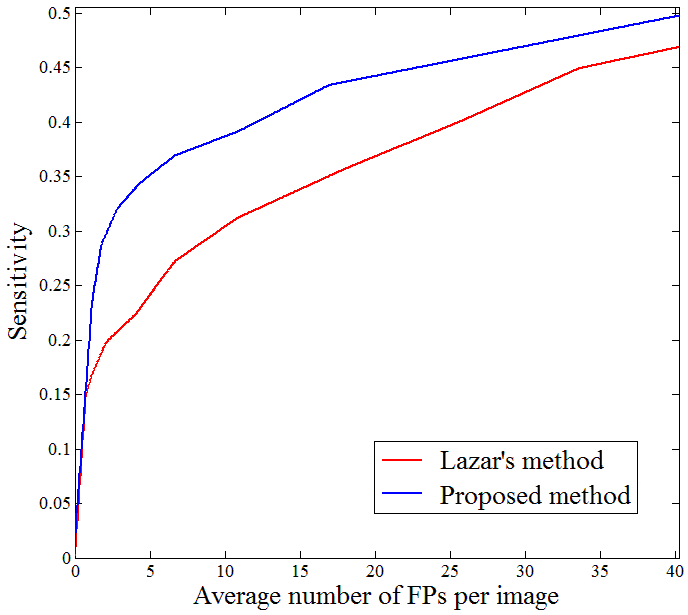

Fig. 6. The FROC curves of the proposed method and Lazar's method.

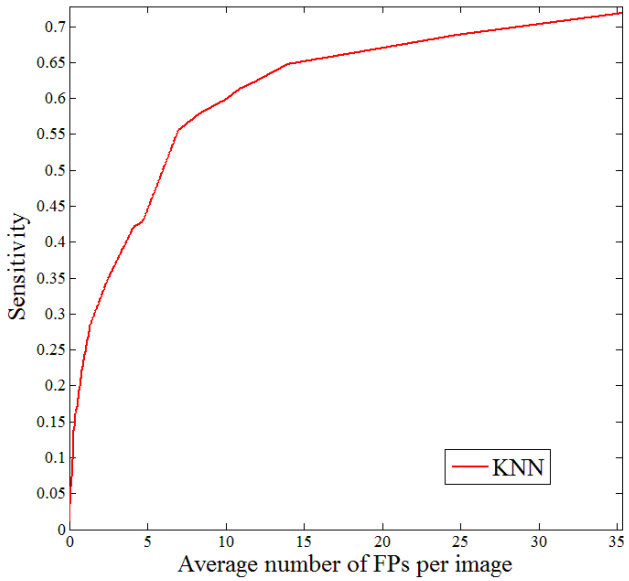

Fig. 7. The FROC curve of proposed method on the public database of e-ophtha-MA.

TABLE Ⅰ SENSITIVITIES AT PREDEFINED FLASE POSITIVE PER IMAGE RATE FOR THE PROPOSED METHOD AND THE LAZAR'S METHOD IN THE ROC DATABASE

	1/8	1/4	1/2	1	2	4	8
Lazar's method	0.037	0.055	0.103	0.162	0.196	0.223	0.285
Proposed method	0.037	0.056	0.103	0.206	0.295	0.339	0.376

TABLE Ⅱ SENSITIVITIES AT PREDEFINED FLASE POSITIVE PER IMAGE RATE FOR THE PROPOSED METHOD IN THE E-OPHTHA-MA DATABASE

	1/8	1/4	1/2	1	2	4	8
Proposed method	0.063	0.117	0.172	0.245	0.323	0.417	0.573